Spatial Modeling of Hydrocarbon Productivity in the Nahr Umr Formation at the Luhais Oil Field, Southern Iraq

Amna M. Handhal, Amjad A. Hussein, Alaa M. Al-Abadi & Frank R. Ettensohn

Natural Resources Research
Official Journal of the International Association for Mathematical Geosciences

ISSN 1520-7439

Nat Resour Res
DOI 10.1007/s11053-020-09751-y

Springer

Natural Resources Research (© 2020)
https://doi.org/10.1007/s11053-020-09751-y

Original Paper

Spatial Modeling of Hydrocarbon Productivity in the Nahr Umr Formation at the Luhais Oil Field, Southern Iraq

Amna M. Handhal,[1,2] Amjad A. Hussein,[1] Alaa M. Al-Abadi,[1,2,3] and Frank R. Ettensohn[1,2,3]

Received 29 June 2020; accepted 18 September 2020

In this study, a trial exercise was performed for the first time to model the productivity of a reservoir unit, using a GIS-based hybridization of Shannon's entropy method and the technique for order preference by similarity to an ideal solution (TOPSIS) approach. A case study from the middle reservoir unit of Nahr Umr Formation in the Luhais oil field in southern Iraq was used to demonstrate the benefits of the proposed methodology in managing hydrocarbon reservoirs with cost-effective modeling techniques. The heterogeneity of the reservoir unit was firstly quantified using the Lorenz coefficient (L_k) and the Dykstra–Parsons permeability variation (V_k). The average calculated L_k and V_k were 0.65 (heterogeneous) and 0.93 (very heterogeneous), respectively. This stage of the analysis confirmed the heterogeneous nature of the reservoir unit. To overcome the problem reservoir heterogeneity, the hydraulic flow unit (HFU) concept was used. Interactive Petrophysics software was used to create HFUs, and the number of HFUs was optimized using k-means clustering techniques. The estimated number of HFUs was 2. For each HFU, seven petrophysical properties or factors, namely porosity (ϕ), thickness, volume of shale (V_{sh}), bulk volume of water (BVW), total water saturation (SWT), hydrocarbon saturation (Sh), and bulk volume of hydrocarbons (BVH), were calculated for each well location based on well logs and core data availability. The ordinary kriging technique was used to interpolate the seven petrophysical properties for each HFU over the study area. Shannon's entropy model was then used to assign factor weights for each HFU. In the case of HFU-1, the calculated weights were 0.218, 0.190, 0.141, 0.132, 0.111, 0.107, and 0.103 for Sh, unit thickness, BVH, BVW, ϕ, SWT, and V_{sh}, respectively. For HFU-2, the calculated weights were 0.179, 0.178, 0.170, 0.154, 0.146, 0.092, and 0.081, for V_{sh}, BVH, Sh, SWT, unit thickness, BVW, and ϕ, respectively. The TOPSIS algorithm was then implemented using *R* statistical software, and ranked values from the TOPSIS were interpolated using the ordinary kriging technique to reveal the spatial distribution of hydrocarbon productivity after division into three productivity zones: low, moderate, and high. For HFU-1, these zones

[1]Department of Earth and Environmental Sciences, University of Kentucky, Lexington, USA.
[2]Department of Geology, College of Science, University of Basrah, Basrah, Iraq.
[3]To whom correspondence should be addressed; e-mail: Alaa.Al-Abadi@uky.edu, alaa.atiaa@uobasrah.edu.iq, fettens@uky.edu

Published online: 28 September 2020

encompass 32, 22, and 45 km^2 for the low-, moderate-, and high-productivity zones, respectively. For HFU-2, these zones cover 30, 23, and 46 km^2, respectively. The promising high-productivity zone for HFU-1 was concentrated in the southern and northern parts of the unit; for HFU-2, the high-productivity zone occupies a northeast–southeast-oriented swath in the middle part of the unit. In general, the lower part of the middle Nahr Umr Formation, represented by HFU-2, is more productive than the upper part, representing HFU-1. The model results were validated using 42 productive well locations in the study area, and results indicated that the developed models performed well with 76% and 88% accuracy for HFU-1 and HFU-2, respectively. The hydrocarbon productivity maps produced by the techniques developed herein can be used by reservoir managers, geologists, and reservoir engineers as guides for drilling new, productive wells with minimum effort and cost.

KEY WORDS: Flow units, Heterogeneity, Iraq, Nahr Umr formation, Spatial modeling.

INTRODUCTION

Spatial analysis (SA) is one of the most important tools in geographic information systems (GIS). Using this tool, information can be combined from many independent and diverse sources, and new information can be extracted by applying a complex set of spatial operators (Goodchild 2005). Through operators for SA, complex questions can be answered concerning spatial relationships. It is also possible to define the patterns of occurrence of different phenomena, in addition to analyzing layers (thematic maps), to determine the suitability of a place for a specific activity (Maguire et al. 2005). Tools for SA also enable us to address critically important questions and decisions that are beyond the scope of simple visual analysis. The process of integrating SA with advanced statistical techniques, multi-criteria decision-making (MCDM), soft computing, and machine learning models has opened broad prospects for research around the world, including the study landslide susceptibility (Chen et al. 2018; Dou et al. 2019; Nohani et al. 2019), flood susceptibility mapping (Al-Abadi and Al-Najar 2019; Janizadeh et al. 2019), gully erosion (Al-Abadi and Al-Ali 2018; Arabameri et al. 2019; Azareh et al. 2019), as well as groundwater potential and spring potential mapping (Al-Abadi et al. 2019; Bui et al. 2019; Kordestani et al. 2019). In the field of petroleum geology and petroleum exploration, many researchers have tried to use SA to analyze hydrocarbon potential (Alshayef et al. 2019; Amiri et al. 2015), discover new hydrocarbon sources (Gao et al. 2000; Chen and Osadetz 2005; Bingham et al. 2012), and discern hydrocarbon migration pathways (Liu et al. 2008; Rudini Matori et al. 2018).

At the level of petroleum reservoir units, no studies using SA are yet available for predicting the best places for high hydrocarbon production, except by seismic surveys, well logging, and the drilling of exploration boreholes, which are very costly in terms of money, effort and time. The problem facing researchers in using SA for hydrocarbon prospecting is the heterogeneous nature of formations penetrated by wells and thus the difficulty of averaging the various petrophysical parameters of the reservoir units, such as porosity and permeability. It is well known that formation characteristics change laterally and with depth, and hence, the use of averaging for quantifying reservoir characteristics will give incorrect results and an incorrect evaluation of hydrocarbon potential for a given reservoir unit. To overcome this problem, the current research suggests using the concept of hydraulic flow unit (HFU), which is a mappable part of the reservoir wherein the geological and petrophysical properties influencing fluid flow are consistent and consistently distinct from those of other reservoir rock units (Ebanks 1987). Therefore, in this study, we propose to map hydrocarbon productivity through integration of SA, MCDM, and the concept of HFU. Hence, the objective is to predict which portion of a reservoir will be the most productive in terms of spatial distribution in order to drill new, successful wells without expending more money and effort using only available core and well log data.

MCDM is a subdiscipline of operations research that explicitly evaluates multiple conflicting criteria in decision-making problems. It is a popular tool in the decision-making world, because it improves the ability of decision-makers to make decisions by considering all the criteria and objectives simulta-

neously (Al-Abadi et al. 2018). Despite its use in many scientific, engineering, social, and economic fields, the use of MCDM in petroleum-related problems is still very limited. Many MCDM techniques have been developed in the past few decades, and they can be classified according to the type of decision model that is applied to the situation (Polatidis et al. 2006). Of all the MCDM techniques available today, the analytical hierarchy process (AHP) and the technique for order preference by similarity to an ideal solution (TOPSIS) are the most applied methods in the earth sciences and natural hazard assessment. Thomas L. Saaty created AHP in the 1970 s as a systematic framework for organizing and evaluating complex decisions, and AHP provides an adaptable, low-cost and understandable output for complex decision-making (Wind and Saaty 1980). Given its versatility and ease of implementation and interpretation, AHP largely relies on an expert's opinion of the weighting of criteria, which is the major source of uncertainty (Al-Abadi et al. 2018). To avoid this subjectivity in assessing the relative weights of attributes, this study proposes to use Shannon's entropy concept (Shannon 1948). Entropy is utilized for measuring the degree of disorder in a system (Yue 2017). The entropy concept in information theory can be understood as a measure of the degree of uncertainty expressed by a discrete probability distribution (Hafezalkotob and Hafezalkotob 2016). The entropy concept can be used efficiently in the decision-making process because it tests existing contrasts between datasets and explains the average intrinsic knowledge transmitted to decision-makers. On the other hand, TOPSIS is a powerful method for testing alternatives, which was originally proposed by Hwang and Yoon (1981). TOPSIS chooses alternatives that have the shortest geometric distance from the positive ideal solution and the longest geometric distance from the negative ideal solution (Assari and Assari 2012).

The current research aims mainly to present a new methodology for managing reservoir units and determining the best places to drill productive hydrocarbon wells by integrating SA, TOPSIS, entropy, and the concept of HFU. The middle reservoir unit of Nahr Umr Formation in Luhias oil field in southeastern Iraq (Fig. 1) was chosen as a case study to demonstrate the potential of these techniques in solving some difficult issues in the field of hydrocarbon reservoir management.

STUDY AREA

The Luhias oil field is located in the Basra Governorate, close to the administrative borders of Nasiriyah Governorate, 105 km west of the Basra Governorate center and 100 km southwest of the giant North Rumaila oil field. The field is 20 km long and 5 km wide in the northern part of the field and 10 km wide in the southern part (van Bellen et al. 1959). The shape of the structure appears to be amebic as no specific axis is apparent for the structure (Fig. 1). From a tectonic point of view, the field is located in a formerly unstable shelf zone, the Zubair subzone (Idan et al. 2019), which is considered to be the southern part of the Mesopotamian zone, a Cenozoic foreland basin formed between the colliding Arabian and Iranian plates (Jassim and Goff 2006; Fouad 2010; Darweesh et al. 2017). The Zubair subzone is bordered on the north by the transverse (NE–SW) Takhadid-Qurna fault and on the south by the transverse (NE–SW) Al-Batin fault in the Basra district (Darweesh et al. 2017). The region was probably uplifted during the Hercynian deformation, which took place from Late Devonian through Middle Permian time, but subsequently subsided through Late Permian time (Jassim and Goff 2006). Most of the oil fields in southern Iraq (including Luhais oil field) were formed as a result of the impact of the Arabian Plate with parts of the Iranian plate to the north and east during Oligocene time. The resulting compression affected the form of depositional layers in the basins along the northeastern edge of the Arabian Plate, including the Mesopotamian foreland basin, resulting in broad folds that later became large oil traps (Abdullah et al. 1997). It is also believed that the Luhais structure formed along lineation developed during the eruption of the Neoproterozoic–Cambrian (Infracambrian) Hormuz Salt Formation (Husseini 1988; Rad et al. 2008), which continued through Jurassic time. The collision of Arabian and Iranian plates contributed to the final form of the field in Miocene–Pliocene time (Aqrawi et al. 2010).

The Nahr Umr Formation, the target of this study, is a sandstone reservoir initially defined by Glynn Jones in 1948 from the Nahr Umr structure in southern Iraq (Abid et al. 2015). In its type area in southern Iraq, it comprises black shale interbedded with medium- to fine-grained sandstones with lignite, amber, and pyrite (Owen and Nasr 1958). The sandstone is locally sealed by shales beneath the Mauddud

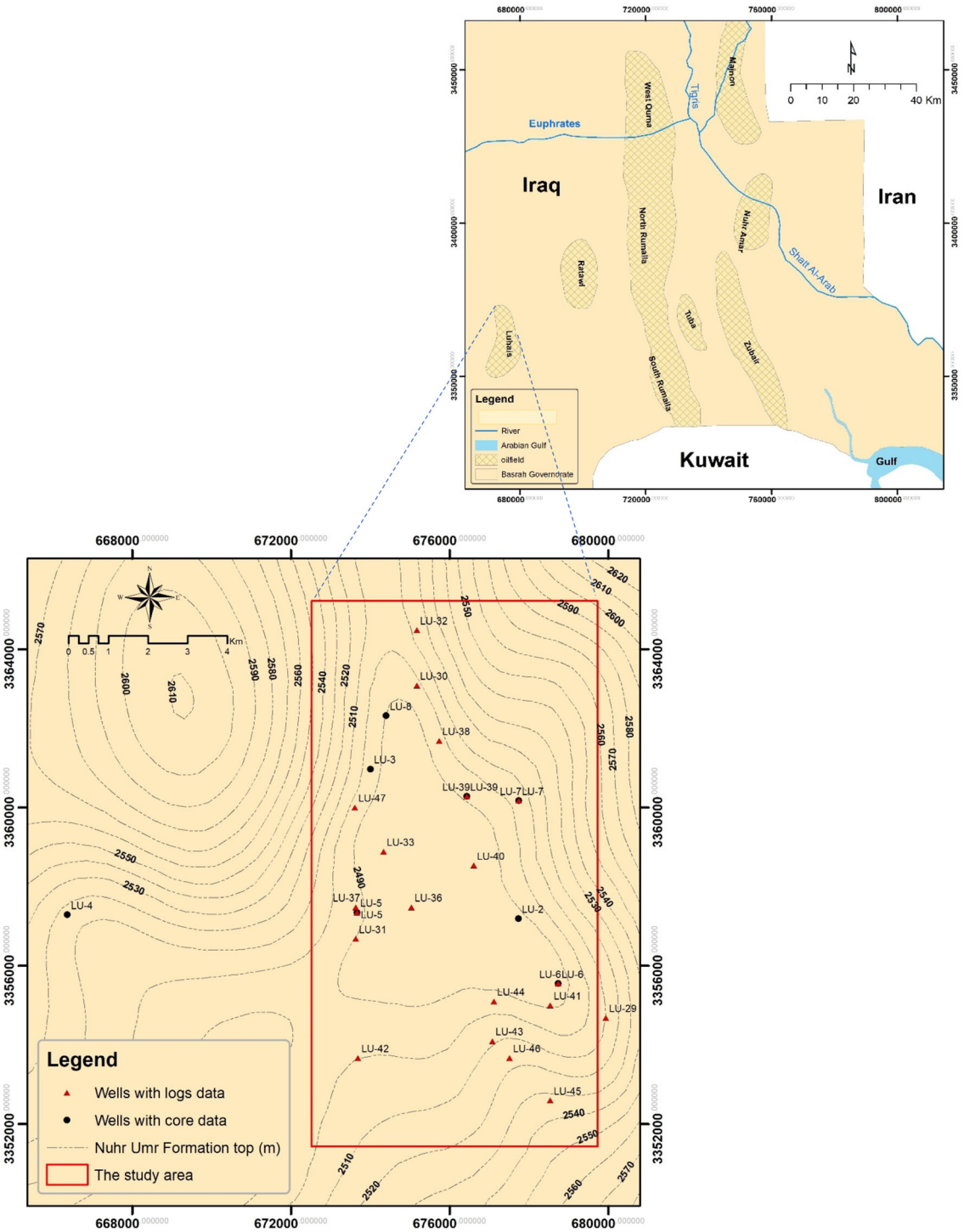

Fig. 1. Location of the study area in southeastern Iraq.

Formation (Al-Naqib 1967). According to Dunnington et al. (1959), a carbonate unit occurs locally in the upper part of Nahr Umr Formation in southern Iraq, pinching out to the west and south. The formation is Late Aptian–Albian in age, and depositional environments include alluvial to lower coastal plain to deltaic deposits with shallow marine and eolian influences (Ibrahim 1983). According to the general division and the definition given by van Bellen et al. (1959), the lower boundary of the formation in the type area is harmonious and gradual, and the surface of disconformity also appears in the Dujaila area and was accepted by (Ditmar and Team 1972), who found that the top boundary was also conformable. The Mauddud Formation constituted the upper boundary of the Nahr Umr in a conformable and gradual manner. The Dolomite Limestone may rise in the Mauddud Formation base of the top of sandstone or layers of shale to the Nahr Umr Formation. The formation of the bottom is a non-conformable surface with Shuaiba Formation, which represents layers of foliate dark black shale to the base Nahr Umr Formation or at the top of the layers of yellow Dolomite or pale gray for Shuaiba Formation (Qaradaghi et al. 2008). The Nahr Umr Formation is equivalent to the upper part of the Sarmord Formation in northern Iraq (Al-Naqib 1967). It is equivalent Burgan Formation in Kuwait, which is located in southeastern Iraq (Owen and Nasr 1958). It is also equivalent to Khafji and Safaniya Formations in northern Saudi Arabia (Powers 1968). It is also equivalent to the Lower Kadhmi Formation in southern of Iran (James and Wynd 1965). The formation in the Luhais oil field in southern Iraq has been divided into two members: a shale member and a sand member. The thickness of the formation is more than 360 m in the southern part of the Salman and Mesopotamian zone. The thickness of the formation in Iraq and Kuwait reaches up to about 400 m, while in the south of Baghdad and northwestern of Iraq it is down to 160 m (Jassim and Goff 2006).

Based on the qualitative and quantitative interpretation of conventional well log data, the Nahr Umr Formation can be divided into three reservoir units of sandstone with smaller amounts of interbedded shale, separated by two prominent shale layers, thereby dividing the formation into the upper, middle, and lower reservoir units (Fig. 2). The middle reservoir unit is the target of this study, because it represents the most promising reservoir in the Nahr Umr Formation. This unit is predominantly composed of porous sandstone layers with interbedded shale layers. The average thickness of this unit is $\sim$ 45 m.

MATERIALS AND METHODS

Mapping of hydrocarbon productivity, the objective of this study, was accomplished in the following six steps (Fig. 3). (1) Available data were gathered from core and well logs for the considered reservoir unit. (2) Using porosity and permeability acquired from the core data for seven wells (Lu-2, Lu-3, Lu-4, Lu-5, Lu-7, Lu-8, and Lu-39), the degree of heterogeneity for the given reservoir unit was quantified using the Lorenz coefficient L_k and the Dykstra–Parsons permeability variation V_k. (3) Based on the results of step 2, a decision was made to use or not to use the HFU to overcome heterogeneity problems. (4) The factors affecting hydrocarbon productivity were determined from the interpretation of logs and core data for each HFU identified in step 3 and include average porosity (ϕ), thickness, volume of shale (V_{sh}), bulk volume of water (BVW), total water saturation (SWT), hydrocarbon saturation (Sh), and bulk volume of hydrocarbons (BVh). (5) The hydrocarbon potential of each HFU was then quantified using a hybrid MCDM and Shannon's entropy method to reveal potential sites for drilling productive wells. Finally, (6) model results were validated by direct comparison with the current productive wells.

Data Used

Data available from the Basrah Oil Company (BOC) for the middle reservoir unit of the Nahr Umr Formation were used to complete the study. The available data included the ϕ and permeability (k) measured from core data for seven wells (Lu-2, Lu-3, Lu-4, Lu-5, Lu-7, Lu-8, and Lu-39). The total number of cores available was 313. Table 1 provides a statistical summary of the available ϕ and k, from which it can be concluded that both parameters are skewed (Fig. 4). The values of ϕ (C_V = 0.3) show more variation than the values of k (C_V = 1.55). The ϕ ranged from 0.025 to 0.292 with an average 0.194, while k ranged from 0 to 6522 md with an average

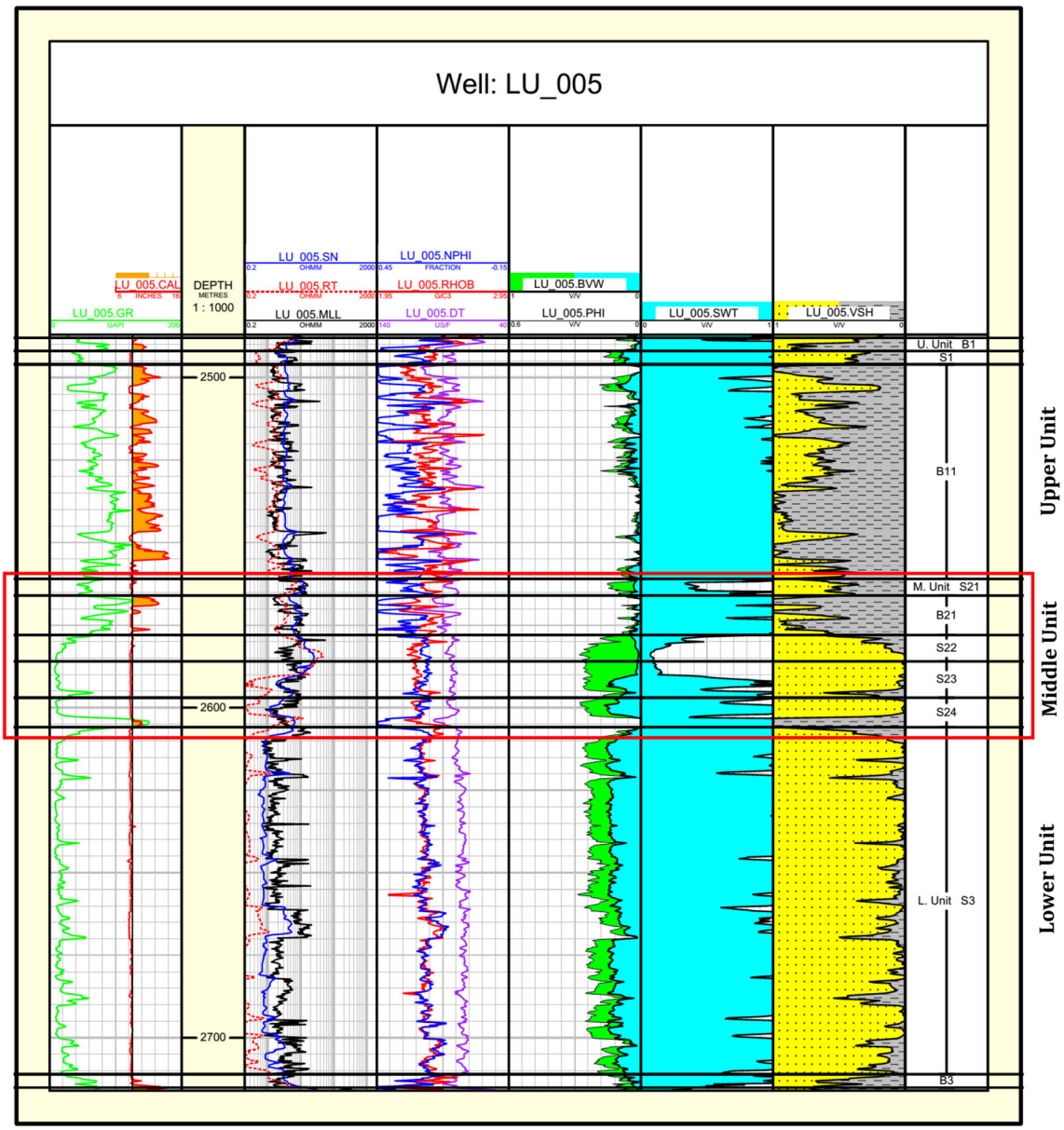

Fig. 2. Computer-processed interpretation (CPI) of LU- 005 in the Luhais oil field (Nahr Umr Formation).

540 md. The available data also included the well log data from twenty wells (Lu-5, Lu-6, Lu-7, Lu-39, Lu-18, Lu-29, Lu-30, Lu-32, Lu-33, Lu-36, Lu-37, Lu-38, Lu-40, Lu-41, Lu-42, Lu-43, Lu-44, Lu-45, Lu-46, and Lu-47). The available well log types included gamma-ray, resistivity, sonic, density, and neutron. The following parameters were deduced from well log data: ϕ, reservoir unit thickness, V_{sh}, BVW, SWT, Sh, and BVh. A detailed description of these factors and how they can be calculated is found in Ellis and Singer (2007) and Liu (2017).

Techniques Used

Reservoir Heterogeneity

Reservoir heterogeneity (RH) is a term used to characterize a reservoir's geological complexity and the relationship of its complexity to the contained fluids (Handhal 2016). Variations in various geological processes like erosion, deposition, lithification, folding, and faulting dictate the heterogeneity and non-uniformity of the reservoir rocks (Tiab and

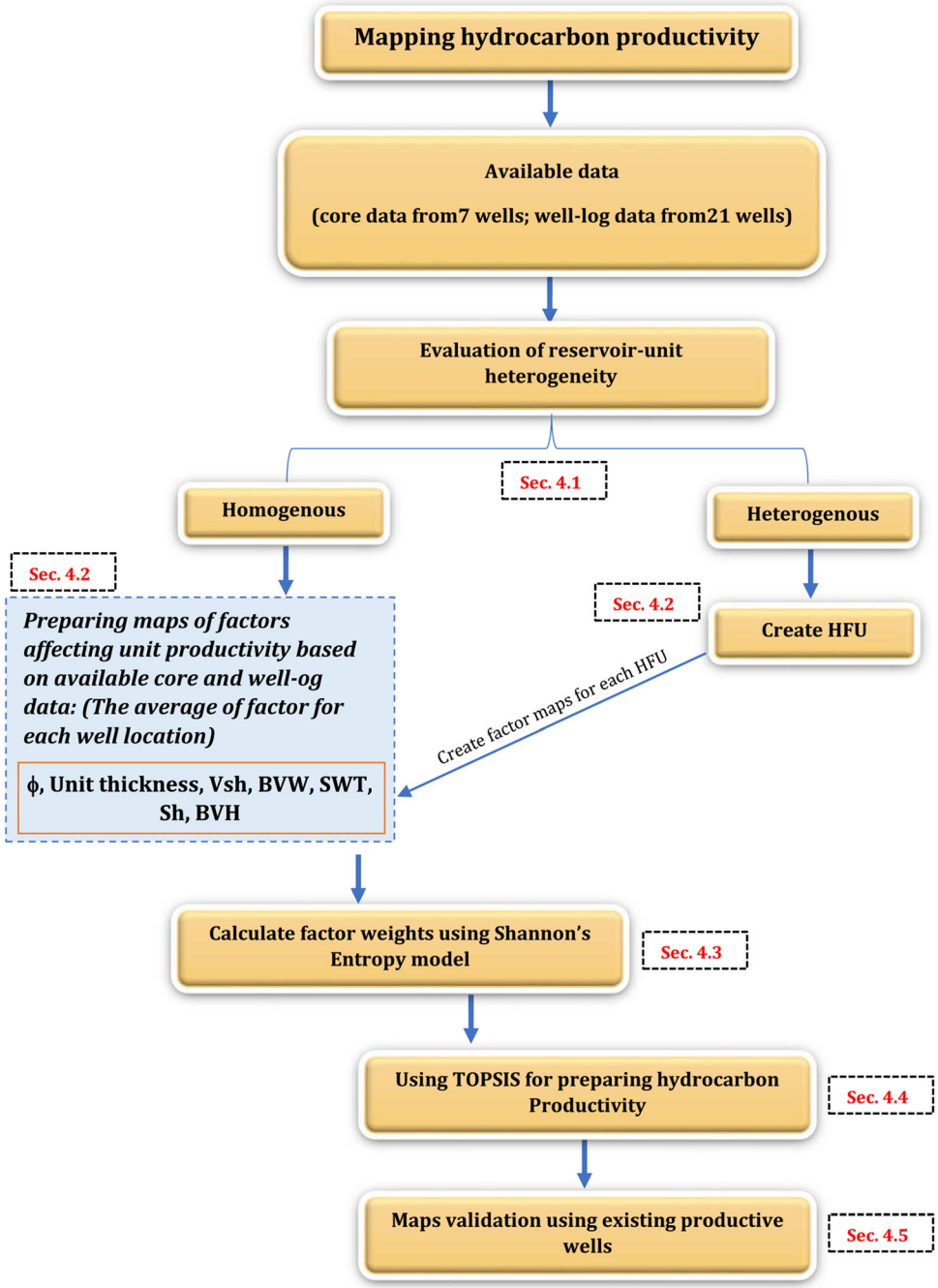

Fig. 3. Steps followed in this study.

Donaldson 2015). A quantitative evaluation of RH is important for predicting reservoir performance during waterflooding, designing an efficient injection production system, maximizing hydrocarbon production, and understanding the salient conditions that are homogenous in the petroleum reservoirs. In general, the two widely used statistical measures to quantify the degree of RH are the Lorenz coefficient L_k and the Dykstra–Parsons permeability variation V_k (Tiab and Donaldson 2015). L_k is a measure of heterogeneity that takes into account the statistical nature of the porosity and permeability in a strati-

Table 1. Statistical summary of porosity (fraction) and permeability (md) derived from core data

Well no.	Statistical measures							
	Parameter	Core No.	Min.	Max.	Mean	Sd	C_V	Skewness
Lu-2	ϕ (fraction)	79	0.030	0.276	0.204	0.063	30.75	− 1.48 (HS)
	k (md)	79	0.000	6522	919	1264	137.63	2.09 (HS)
Lu-3	ϕ (fraction)	82	0.025	0.256	0.196	0.051	26.29	− 1.88 (HS)
	k (md)	82	0.200	1355	290.4	297.9	102.59	1.60 (HS)
Lu-4	ϕ (fraction)	34	0.0790	0.273	0.187	0.067	35.81	− 0.33 (S)
	k (md)	34	0.000	2210	401	616	153.71	1.98 (HS)
Lu-5	ϕ (fraction)	24	0.045	0.239	0.175	0.048	27.79	− 1.57 (HS)
	k (md)	24	0.000	2800	331	605	182.68	3.31 (HS)
Lu-7	ϕ (fraction)	47	0.043	0.264	0.186	0.055	30.08	− 0.73 (HS)
	k (md)	47	0.2	1869	367	408.9	111.32	1.37 (HS)
Lu-8	ϕ (fraction)	34	0.062	0.292	0.205	0.062	30.25	− 1.00 (S)
	k (md)	34	0.000	2329	615	594	96.52	0.97 (S)
Lu-39	ϕ (fraction)	13	0.094	0.262	0.179	0.060	33.53	− 0.10 (S)
	k (md)	13	0.000	4950	994	1455	146.37	1.87 (HS)
All core data	ϕ (fraction)	313	0.025	0.292	0.194	0.058	30.13	− 1.07 (S)
	k (md)	313	0.000	6522	540	540	155.46	3.19 (HS)

Sd: standard deviation; Cv: coefficient of variation; HS: highly skewed; S: skewed

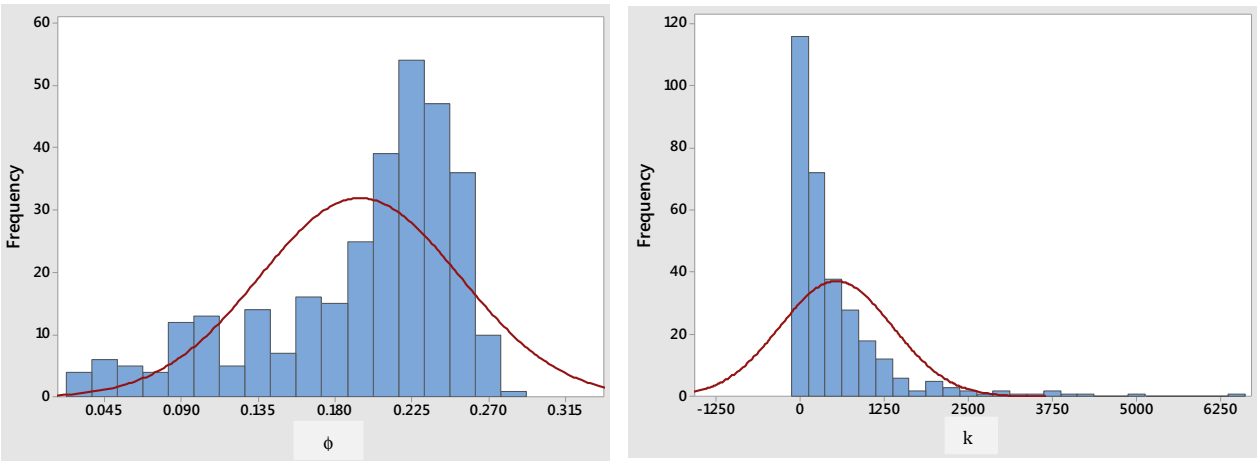

Fig. 4. Histogram of ϕ and k from core data.

fied reservoir and is calculated by plotting the product of average permeability and reservoir unit thickness (cumulative flow capacity) on the y-axis versus the product of average porosity and thickness for the same reservoir unit (cumulative storage capacity) on the x-axis. The value of L_k ranges from 0 to 1. A reservoir is said to be homogenous if L_k approaches 0, and it is extremely heterogeneous if L_k approaches 1. V_k, on the other hand, is a dimensionless measure of sample variability or dispersion (Jensen et al. 2000). V_k is obtained by plotting permeability values on a log probability curve to obtain the values at certain probabilities and then placing those values into the following equation:

$$V_k = \frac{k_{50} - k_{84.1}}{k_{50}} \quad (1)$$

where k_{50} is the permeability value at 50% probability and $k_{84.1}$ is the permeability value at 84.1% probability of occurrence in the cumulative sample. The range of V_k is from 0 to 1. A reservoir is said to be homogeneous, slightly heterogeneous, heterogeneous, very heterogeneous, extremely heterogeneous, and perfectly heterogeneous if its V_k is 0, 0–

0.25, 0.25–0.5, 0.5–0.75, 0.75–0.99, and 1, respectively.

Hydraulic Flow Units

A HFU is characterized as a stratigraphically continuous interval of similar reservoir operation, which honors the geological structure and retains the rock-type characteristics (Gunter et al. 1997). Hearn et al. (1984) introduced the concept of HFU to determine the distribution of rock types that most strongly control fluid flow. They defined a HFU as reservoir zone, which is continuous both laterally and vertically and has similar permeability, porosity, and bedding characteristics. Amaefule et al. (1993) developed a HFU identification technique based on microscopic measurements of core rock samples that provide parameters for use in the modified Kozeny–Carman equation (Eq. 2) and in the hydraulic mean radius concept (Tiab and Donaldson 2015; Tiab and Donaldson 2015); thus,

$$k = \left(\frac{1}{K_T s_{V_{gr}}^2}\right)\left(\frac{\phi_e^3}{(1-\phi_e)^2}\right) \tag{2}$$

where k is permeability in μm^2, ϕ_e is effective porosity, $s_{V_{gr}}$ is specific area per unit grain volume, K_T is effective zoning factor, and τ is tortuosity of the flow path. By dividing both sides of Eq. (2) by k and taking the square root, we get:

$$\sqrt{\frac{k}{\phi}} = \frac{1}{S_{V_{gr}}\sqrt{K_T}}\left(\frac{\phi}{1-\phi}\right) \tag{3}$$

If k and ϕ are expressed in md and fraction, respectively, the left-hand side of Eq. (3) becomes:

$$\mathrm{RQI} = 0.0314\sqrt{\frac{k}{\phi}}, \tag{4}$$

where RQI is reservoir quality index and is measured in μm. The flow zone indicator (FZI) is defined as:

$$\mathrm{FZI} = \frac{1}{S_{V_{gr}}\sqrt{K_T}} \tag{5}$$

Therefore, Eq. (2) can be rewritten as:

$$\mathrm{RQI} = \mathrm{FZI}(\phi_z) \tag{6}$$

where $\phi_z = \frac{\phi}{1-\phi}$. Taking the logarithm of both sides of Eq. (6) yields:

$$log(\mathrm{RQI}) = log(\phi_z) + log(\mathrm{FZI}) \tag{7}$$

A log–log plot of RQI versus ϕ_z gives a straight line with a slope. The value of *FZI* is determined as the intercept of the slope at $\phi_z = 1$ (Orodu et al. 2016). Samples on the same straight line have similar pore throat characteristics and therefore form an HFU.

Calculation of Factor Weight Based on Shannon's Entropy Concept

To determine objectively the weight of factors used for mapping hydrocarbon productivity by the entropy approach, the following steps were followed.

(1) Formulate a decision matrix, which consists of factors affecting the hydrocarbon productivity of the reservoir unit, such as, among others, porosity, permeability, and volume of shale.

$$\boldsymbol{X} = \begin{bmatrix} x_{11} & x_{21} & . & x_{1n} \\ x_{21} & x_{22} & . & x_{2n} \\ . & . & . & . \\ x_{m1} & x_{m2} & . & x_{mn} \end{bmatrix} \tag{8}$$

where m is number of factors (criteria) used, and n is number of instances (alternatives) per factor.

(2) Standardize the decision matrix $\boldsymbol{X}$ using the following equations:

$$y_i = \frac{x_{i\max} - x_i}{x_{i\max} - x_{i\min}} \quad \text{(for efficiency type)} \tag{9}$$

$$y_i = \frac{x_{i-} x_{i\min}}{x_{i\max} - x_{i\min}} \quad \text{(for cost type)} \tag{10}$$

where $x_i, x_{i\min}, x_{i\max}$ are original, minimum, and maximum i values, respectively. The standardized matrix Y is then written as:

$$\boldsymbol{Y} = \begin{bmatrix} y_{11} & y_{21} & . & y_{1n} \\ y_{21} & y_{22} & . & y_{2n} \\ . & . & . & . \\ y_{m1} & y_{m2} & . & y_{mn} \end{bmatrix} \tag{11}$$

(3) Normalize $\boldsymbol{Y}$ to obtain the project outcomes (P_{ij}) as:

$$P_{ij} = \frac{y_{ij}}{\sum_{i=1}^{m} y_{ij}} \tag{12}$$

(4) Compute the entropy measure of project outcomes via:

$$e_j = -k \sum_{i=1}^{m} P_{ij} ln P_{ij} \tag{13}$$

where $k = 1/\ln m$.

(5) Calculate the entropy weight (w_j) as:

$$w_j = \frac{1 - e_j}{\sum_{i=1}^{n} (1 - e_j)}. \tag{14}$$

TOPSIS

TOPSIS is a compensatory aggregation approach based on the concept that the best alternative should have the shortest distance from the positive ideal solution (PIS) and the farthest distance from the negative ideal solution (NIS) (Hwang and Yoon 1981). *PIS* is the sum of all the best values that can be accomplished for each attribute, whereas *NIS* comprises all the worst values achieved for each attribute (Siahaan et al. 2018). The steps involved to compute ranked values using TOPSIS are as follows.

(1) The decision matrix (Eq. 8) is first normalized using formula 1

$$r_{ij} = \frac{x_{ij}}{\sqrt{\sum_{i=1}^{n} x_{ij}^2}}, \tag{15}$$

where $i = 1, 2, \ldots,$ mand $j = 1, 2, \ldots, n$;

(2) Create a normalized decision matrix by multiplication the criteria weights w_i and r_{ij}

$$v_{ij} = w_i r_{ij}; \tag{16}$$

(3) Calculate PIS and NIS using the following equations

$$\text{NIS} = \left(\min v_{ij} | j \in \hat{J}\right), \left(\max v_{ij} | j \in \breve{J}\right) \tag{17}$$

where $\hat{J}$ and $\breve{J}$ are the benefit and cost criteria, respectively;

(4) Compute the separations of each alternative from *PIS* and *NIS* using Euclidean distance; thus,

$$S_j^+ = \sqrt{\sum_{i=1}^{n} (v_{ij} - v_i^+)^2} \quad j = 1, 2, \ldots, n \tag{18}$$

$$S_j^- = \sqrt{\sum_{i=1}^{n} (v_{ij} - v_i^-)^2} \quad j = 1, 2, \ldots, n; \tag{19}$$

(5) Compute the relative closeness coefficient to the ideal solution via

$$C_j = \frac{S_j^-}{S_j^+ + S_j^-} \quad j = 1, 2, \ldots, n; \text{ and} \tag{20}$$

(6) Finally, rank the alternatives according to C_j, considering that the best alternative is the one that has the highest C_j.

RESULTS AND DISCUSSION

Heterogeneity Test

Table 2 shows the results of heterogeneity calculations for the current study. It is clear that both L_k and V_k measures proved that the studied reservoir unit is heterogeneous. The averages of calculated L_k and V_k were 0.65 (heterogeneous) and 0.93 (very heterogeneous), respectively. Based on these results, the average reservoir unit characteristics cannot be used to complete the spatial productivity analysis. For this reason, the HFU was used in a later section to try to reduce the vertical variation in reservoir properties in order to build accurate spatial models.

HFU Identification and Factor Preparation

To identify HFUs for the reservoir unit under consideration, Interactive Petrophysics (IP) soft-

Table 2. Heterogeneity tests

Well no.	L_k	Evaluation	V_k	Evaluation
Lu-2	0.58	Heterogeneous	0.88	Very heterogeneous
Lu-3	0.55	Heterogeneous	0.91	Very heterogeneous
Lu-4	0.76	Heterogeneous	0.94	Very heterogeneous
Lu-5	0.70	Heterogeneous	0.92	Very heterogeneous
Lu-7	0.69	Heterogeneous	0.90	Very heterogeneous
Lu-8	0.54	Heterogeneous	0.96	Very heterogeneous
Lu-39	0.73	Heterogeneous	0.99	Very heterogeneous
Average	0.65		0.93	

ware was used in this study. To optimize the number of HFUs, the k-means clustering technique was used. K-means is one of the most frequently used unsupervised ML algorithms for partitioning a given set of data into a set of k groups (k clusters), where k represents the number of groups prespecified by the analyzer (MacQueen 1967). Determining the optimal number for k in a dataset is a crucial issue in the successful application of the k-means technique. Different automatic algorithms were developed to specify the optimal number for k, including direct methods such as Elbow and Silhouette and statistical testing methods such as the Gap statistic. Besides these methods, more than 30 other indices and methods have been developed to identify the optimum number for k using ''majority rule'' by implementing in the NBClust () function of the R statistical software (Charrad et al. 2012). The fviz_nbclust () function in the R package was used to execute Elbow, Silhouhette and Gap statistical methods. The results are shown in Fig. 5. The determined optimal number for k using Elbow, Silhouhette, Gap, and NBClut () functions were 4, 2, 3, and 2, respectively. Therefore, the optimal number for k was taken to be 2. The HFUs identified in this study using two classes are shown in Fig. 6. For each HFU, the average reservoir characteristics (ϕ, reservoir unit thickness, V_{sh}, BVW, SWT, Sh, and BVH) for each well were calculated. For those wells having only well logs, depths of the wells having core data close to these wells were used as guides to determine the reservoir interval. The average reservoir characteristics for the all wells (having core or having only logs) for each HFU were then interpolated using the ordinary kriging (OK) technique to get the surfaces of the factors (Fig. 7). Kriging is a family of estimators used to interpolate spatial data. This family includes ordinary kriging, universal kriging, indicator kriging, probability, disjunctive, and co-kriging (Lefohn et al. 2005). Ordinary kriging is a well-known estimation method that minimizes the error of variance and provides an uncertainty measure as well (Yamamoto 2005). From Fig. 7a, the thickness of HFU-1 ranged from 7 to $\sim$ 40 m. The HFU-1 thickness increases from west to east, and the maximum thickness (22 m) appears in the east side of the study area. In contrast, the thickness of UFU-2 ranged from 11 to 32 m and it is distributed unevenly throughout the study area. The average thicknesses of HFU-1 and HFU-2 were 21 and 24 m, respectively. The minimum, maximum, and average values of ϕ for HFU-1 were 0.038, 0.29, and 0.168, respectively. The northern, middle, and southern parts of the study area had high values, whereas the eastern and western parts had the lowest values (Fig. 7b, upper figure). With respect to HFU-2, the ϕ values ranged from 0.09 to 0.28 with average of 0.185. The ϕ of HFU-2 was generally high in the middle of the unit and it decreased toward western and northern portions (Fig. 7b, lower figure). The minimum, maximum, and average BVW values for HFU-1 were 0.024, 0.086, and 0.048, respectively; for HFU-2, they were 0.012, 0.099, and 0.043, respectively. Spatially, the BVW for HFU-1 was high in the northern part and low in the southern part (Fig. 7c, upper figure); also, it was high in middle of the unit from east to west and low in the remaining parts (Fig. 7c, lower figure). In the case of SWT, the minimum, maximum, and average values were 0.103, 0.930, and 0.443, respectively; for HFU-1, they were 0.074, 0.816, and 0.423, respectively. The low values of the SWT were essentially distributed in the middle part of the study area from south to north in both units, whereas the high values appeared at the eastern and western edges (Fig. 7d). For the V_{sh}, the values of minimum, maximum, and average were 0.0172, 0.755, and 0.288, respectively, for HFU-1 and 0.119, 0.387 and 0.255, respectively, for HFU-2. The spatial distribution of this factor in the two units was different; in HFU-1, the high values appeared in the central and western parts (Fig. 7e, upper figure), whereas in HFU-2, the high values concentrated in the northeastern and southwestern parts of the study area (Fig. 7e, lower plot). In the case of Sh, the high values were distributed approximately with the same pattern in both units in the middle of the study area and with a northwest–southeast trend (Fig. 7f). The minimum, maximum, and average values of Sh for both units were 0.174, 0.820, and 0.557, respectively, for HFU-1, and 0.182, 0.924, and 0.576, respectively, for HFU-2. For the last factor, BVH, high values occurred in the northern and southern parts of the study area and low values encompassed the middle parts of HFU-1 (Fig. 7g, upper figure). In contrast, the high values were distributed through the middle of HFU-2 in the south–north direction (Fig. 7g, lower figure), whereas the low values occupied the remaining parts. The maximum, minimum, and average values of BVH for HFU-1 were 0.007, 0.225, and 0.119, respectively, and 0.041, 0.003, and 0.131, respectively, for HFU-2. In general, the

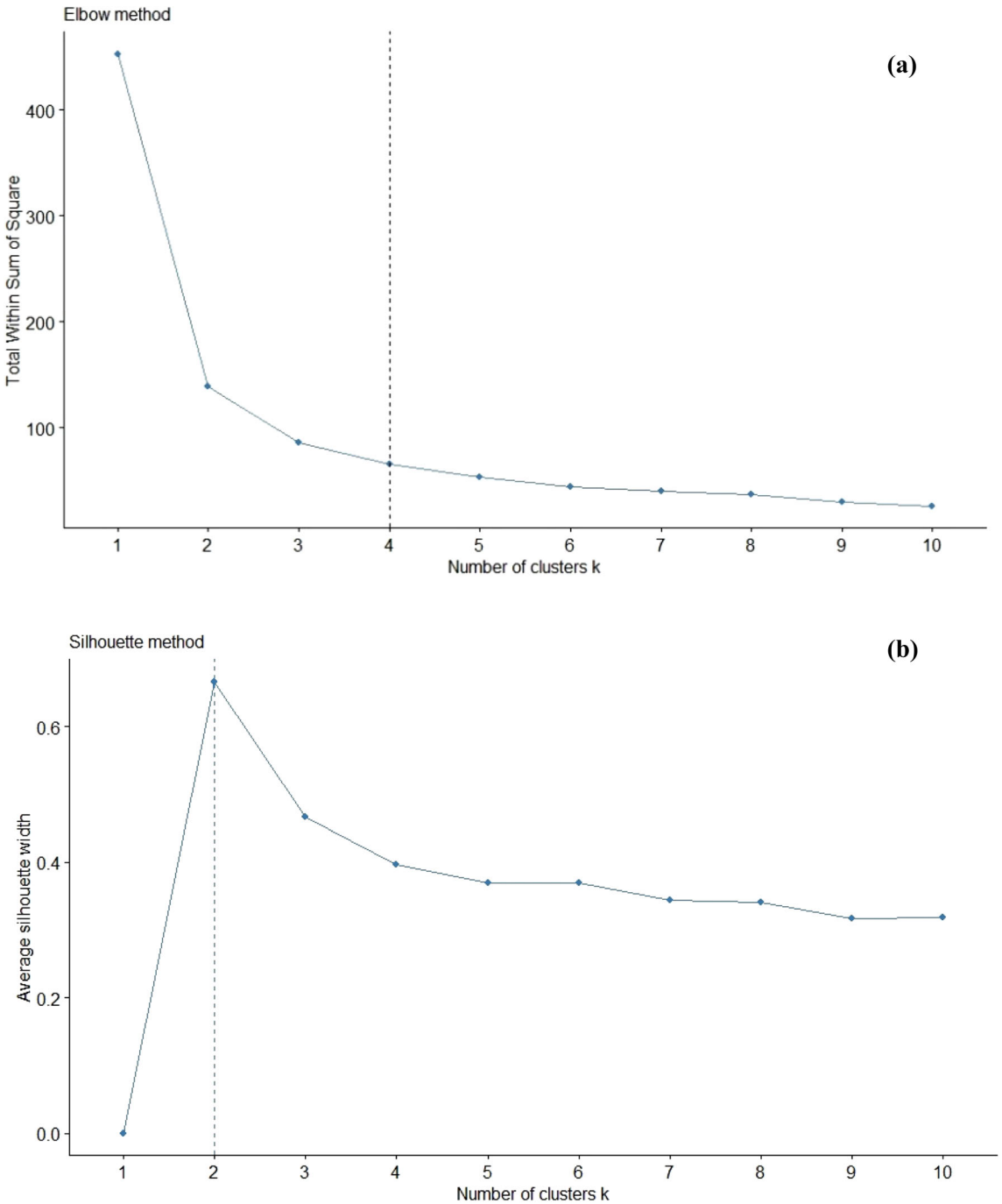

Fig. 5. Number of optimal k using (**a**) Elbow (**b**) Silhouette (**c**) Gap statistic method, (**d**) NBClust function using majority rule of 30 indices.

petrophysical properties that enhanced hydrocarbon productivity (unit thickness, ϕ, Sh, and BVH) in HFU-2 were much better than in HFU-1. Therefore, it should be expected that this unit would be more productive. In addition, high values for these properties were distributed across the

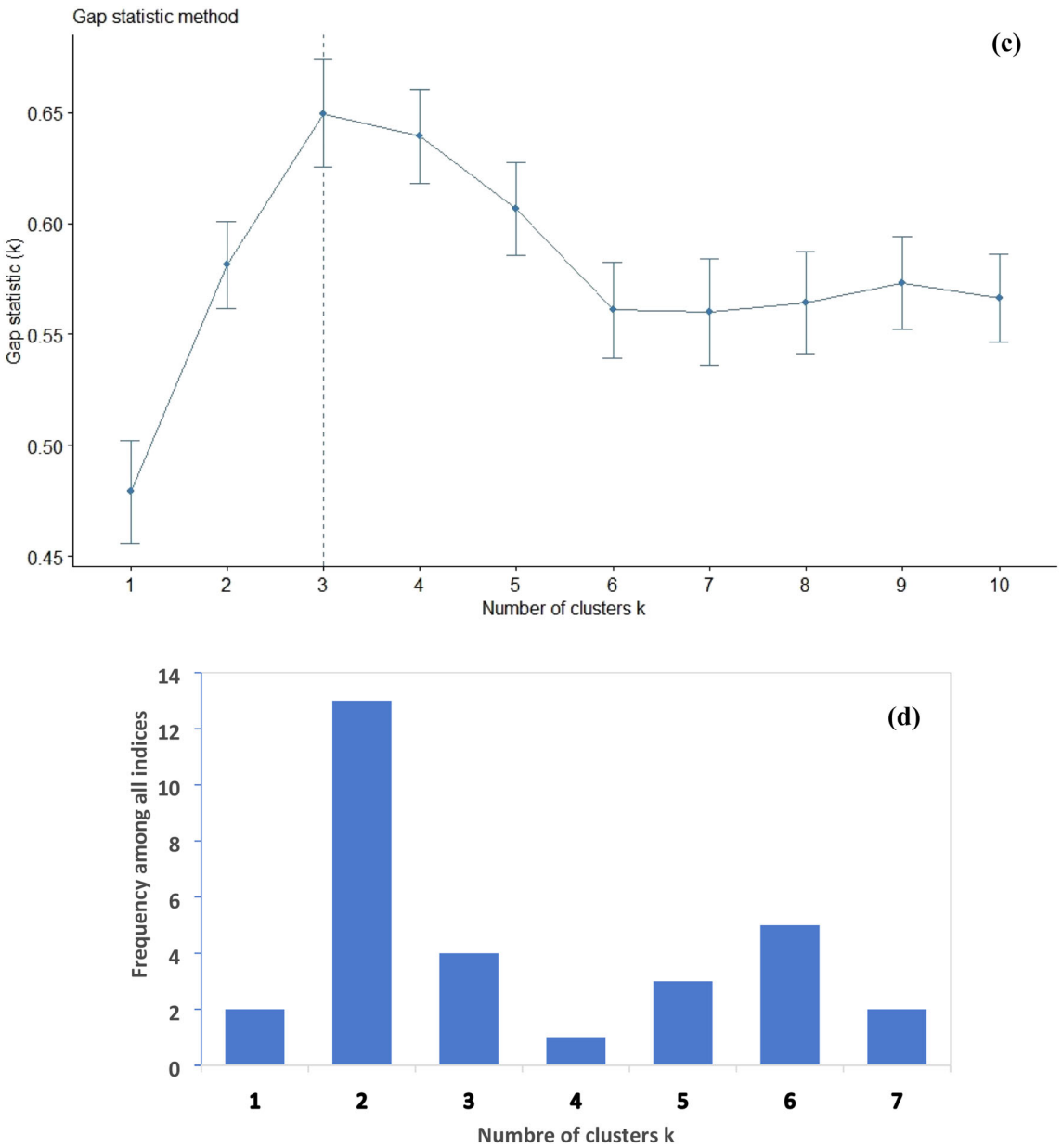

Fig. 5. continued.

middle of the study area in the north–south direction, suggesting that the most promising and productive parts in the middle part of the Nahr Umr Formation run in that direction.

The layers for each factor were prepared as rasters with a 10 × 10 m spatial resolution. The total number of pixels for each factor was 1,440,976, and the number of rows and columns was 904 and 1594, respectively.

Factor Weight Determination

To derive weights using Shannon's entropy model, Eqs. (8)–(14) were used. To standardize factors, the efficiency type (smaller the better), Eq. (9), was used for the V_{sh}, BVW, and SWT. In contrast, the cost type (larger the better), Eq. (10), was used for unit thickness, ϕ, Sh, and BVH. The results of the factor weight calculations using the

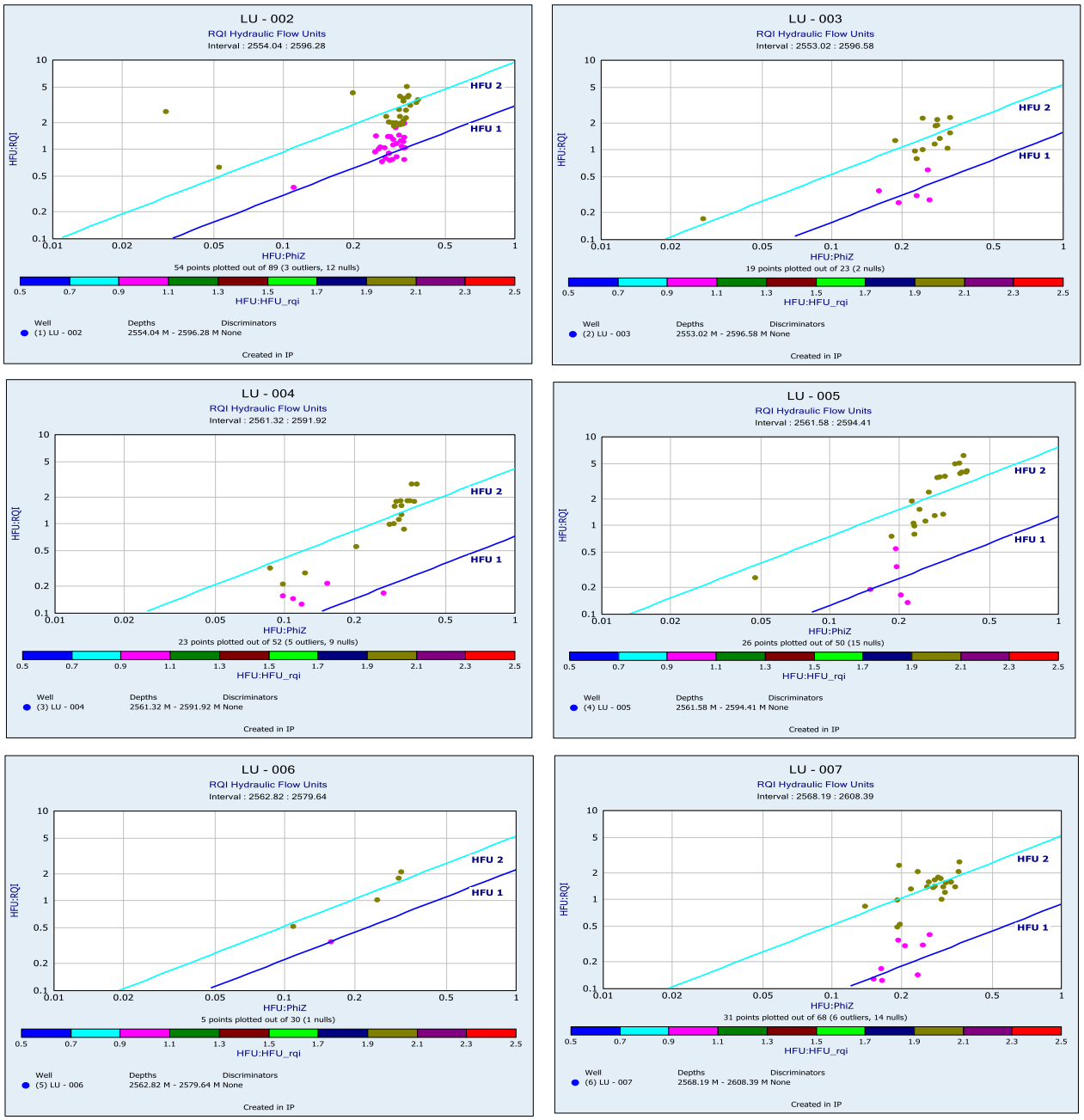

Fig. 6. Flow units.

entropy approach are presented in Table 3 for both HFU-1 and HFU-2. In the case of HFU-1, the higher weights would be allocated in descending order for the Sh (0.218), unit thickness (0.190), BVH (0.141), and BVW (0.132) factors. The V_{sh} has the lowest weight (0.103), followed by SWT (0.107), and then ϕ (0.111). For HFU-2, the V_{sh} has the highest weight (0.179), followed by BVH (0.092), Sh (0.170), and SWT (0.154). The lowest weights were allocated for ϕ (0.081), BVW (0.092), and unit thickness (0.146).

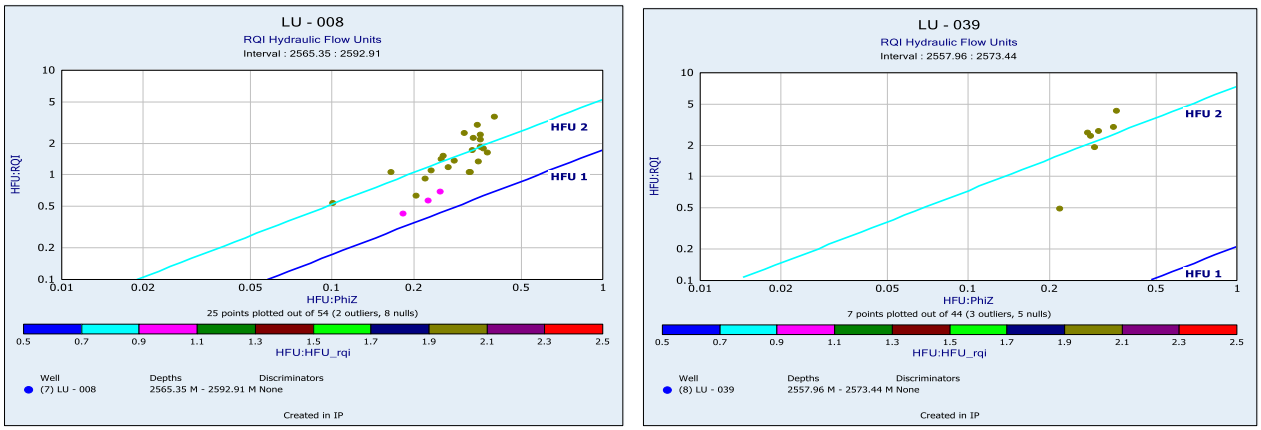

Fig. 6. continued.

TOPSIS RESULTS

To simplify the calculation of rates using the TOPSIS approach, 100 randomly distributed points covering the study area were generated in ArcGIS 10.5 software. Using the "*Extract multi-values to the points*" command, the factor values were extracted for each point and organized in a .csv file. The .csv file, including the factor weights determined in the previous section, was then utilized for rate calculation using the TOPSIS approach by running the "*topsis*" package in the R statistical software. The normalized weighted matrix was prepared using Eq. (16), while Eq. (17) was used to define the PIS and NIS, respectively. The distance to PIS and NIS was determined using Eqs. (18) and (19), and the relative closeness coefficient to the ideal solution of each alternative was obtained using Eq. (20). The C_j calculated through TOPSIS modeling varied from 0.22 to 0.83 for HFU-1 and from 0.12 to 0.89 for HUF-2. These values were used as indices of hydrocarbon productivity, were exported to ArcGIS 10.5, and were interpolated using OK interpolation to reveal the spatial distribution of hydrocarbon productivity in the middle reservoir unit of the Nahr Umr Formation in the Luhais oil field. The interpolated values for hydrocarbon productivity were categorized into three productivity levels using the Jenks natural break (NB) classification scheme (Jenks 1967) (Figs. 8 and 9): low productivity, moderate productivity, and high productivity. With NB, groups were based on the data inherent in the natural groupings. Class breaks were generated in such a way that similar values were better grouped together and the discrepancies between classes were maximized (De Smith et al. 2007). The areas occupied by these three levels for HFU-1 were as follows: 32 km^2, 22 km^2, and 45 km^2 for the low-, moderate-, and high-productivity zones, respectively. In the case of HFU-2, the areas occupied by these same zones were 30 km^2, 23 km^2, and 46 km^2, respectively. The total areas encompassed by the moderate and high levels were 67% and 69%, respectively, of the whole area (99.42 km^2), reflecting the high-productivity conditions of the Nahr Umr middle reservoir unit. In terms of the spatial distribution of the hydrocarbon productivity zones, the promising high-productivity zone for HFU-1 occurs in the southern and northern parts of the study area, whereas low-productivity areas are concentrated in the western and eastern parts of the unit and as a narrow strip in the upper middle part (Fig. 8). In contrast, the high-productivity zone for HFU-2 covers an area running in a northeast–southwest direction across the study area, and the remaining parts encompass a low-productivity zone (Fig. 9). Comparing Figs. 8 and 9 clearly shows that the lower part of the middle Nahr Umr Formation (HFU-2) is more productive than the upper part (HFU-1).

Validation of Results

To validate the maps produced in this study for modeling the spatial productivity of the Nahr Umr middle reservoir unit, the geographic locations of the 41 productive wells in the study area were used

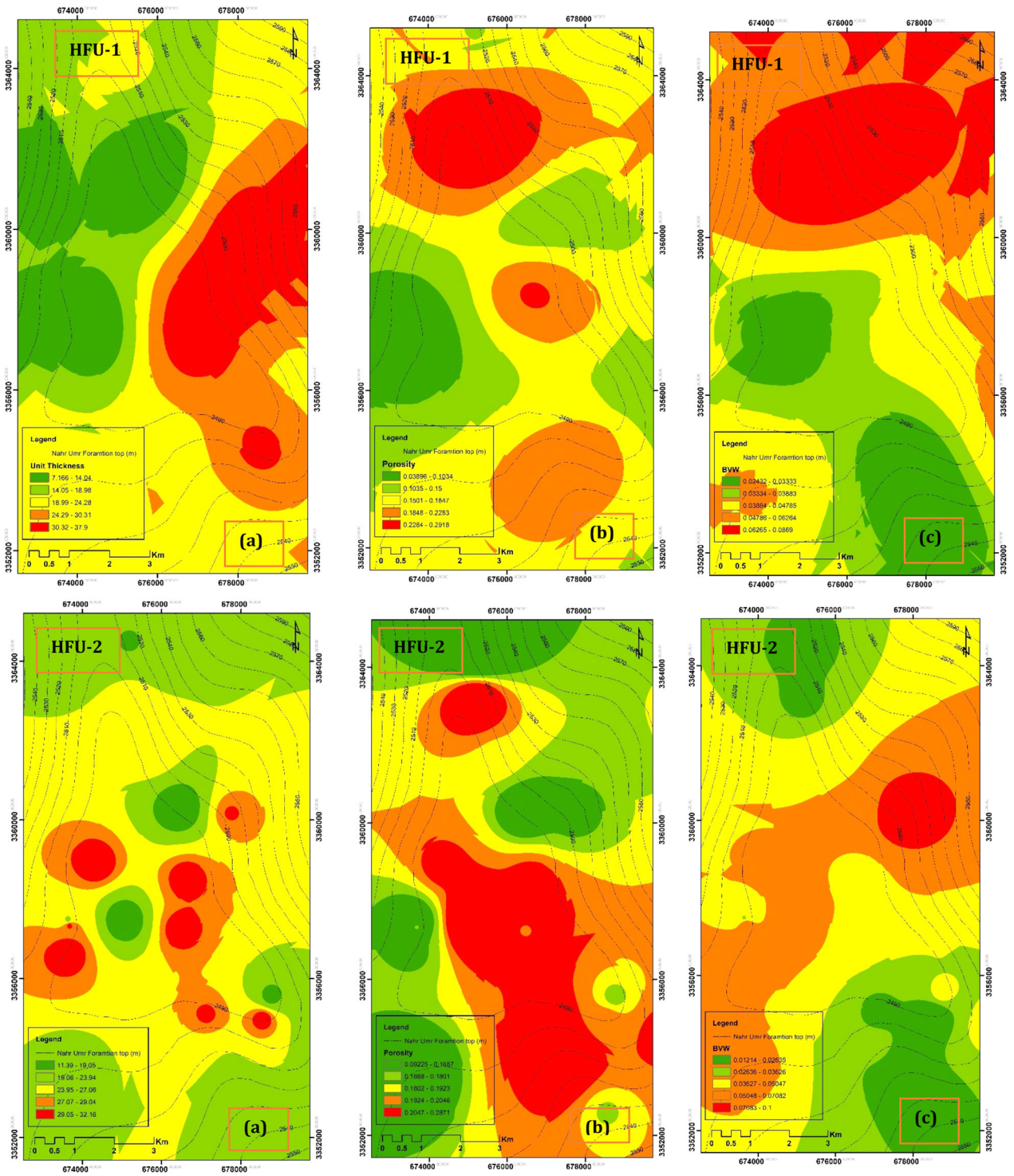

Fig. 7. Factors used in mapping hydrocarbon productivity: (**a**) unit thickness in m; (**b**) porosity (fraction); (**c**) BVW (**d**) SWT (**e**) Vsh (**f**) Sh, (**g**) BVH.

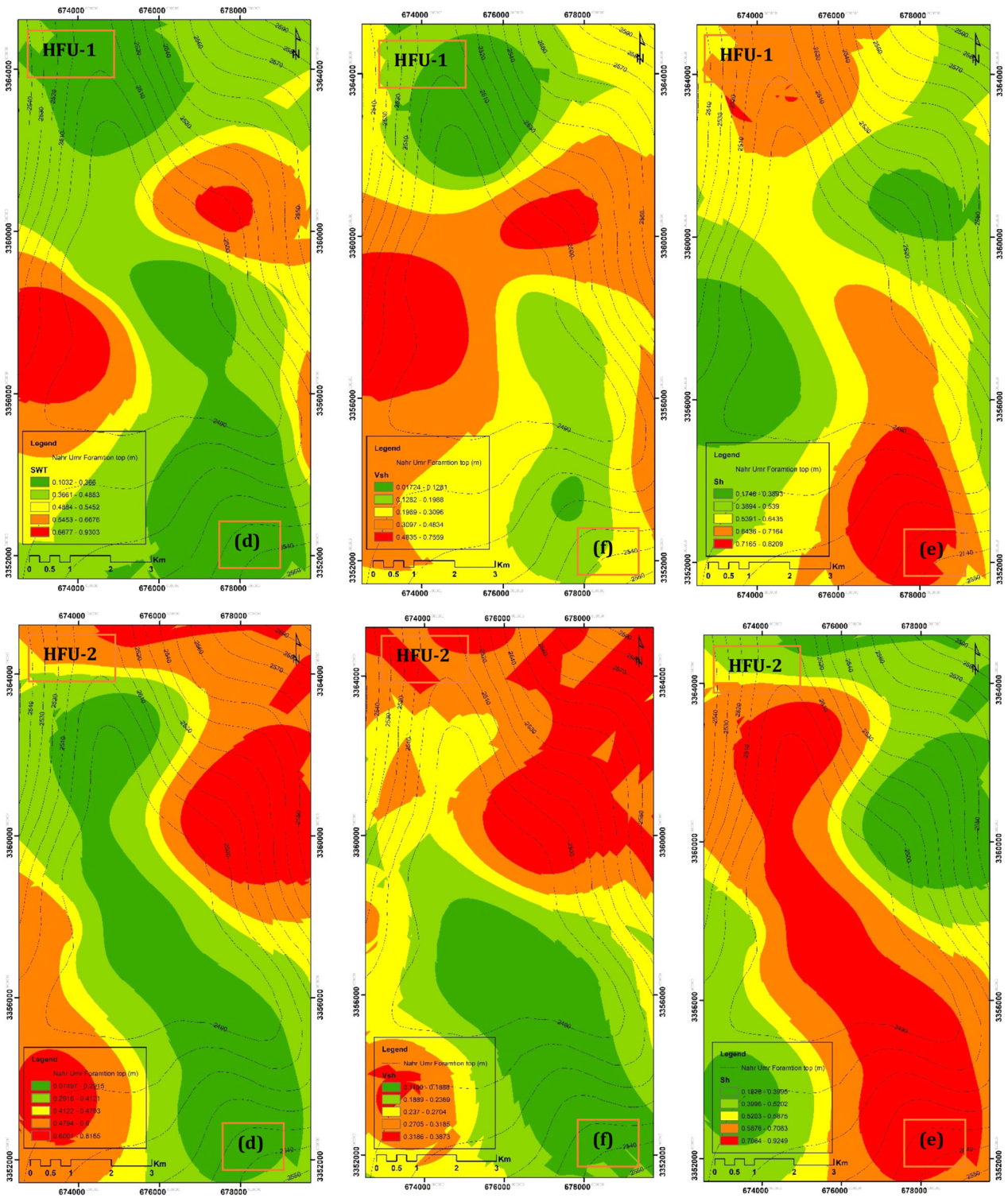

Fig. 7. continued.

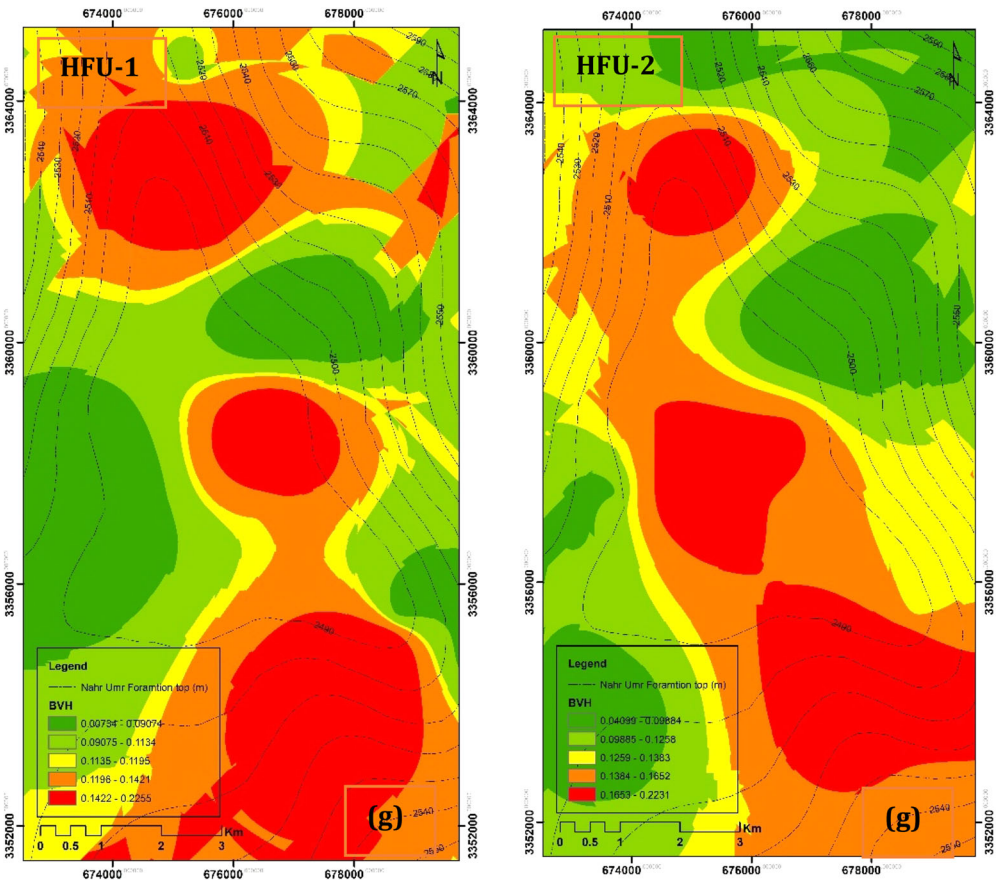

Fig. 7. continued.

as a guide. Direct comparison of the well locations with the derived hydrocarbon productivity zones for HFU-1 and HFU-2 is presented in Fig. 10, from which it is apparent that both models performed well in predicting hydrocarbon productivity zones; the mean accuracy of the models was 76% and 88% for HFU-1 and HFU-2, respectively. The HFU-1 model was successful in predicting hydrocarbon productive zones in 32 well locations (moderate- and high-productivity zones), but failed in nine cases. Similarly, the HFU-2 model predicted the hydrocarbon productivity in 37 well locations, but failed in only four locations. In general, the HFU-2 model was more accurate than the model for the HFU-1.

Table 3. Factor weight calculations using entropy method

Factor	Standardization formula	Calculated weights	
		HFU-1	HFU-2
Unit thickness	Cost	0.190	0.146
ϕ	Cost	0.111	0.081
Sh	Cost	0.218	0.170
BVH	Cost	0.141	0.177
Vsh	Efficiency	0.103	0.179
BVW	Efficiency	0.132	0.092
SWT	Efficiency	0.107	0.154

CONCLUSIONS AND FINAL REMARKS

Despite its widespread use in most sciences and engineering applications, techniques for SA remain almost unknown in the exploration, evaluation, and management of oil and gas reservoirs. This situation is due to the difficulty in carrying out such analyses because of the heterogeneous nature of rock formations in which hydrocarbons occur. To overcome the heterogeneity problem, this study suggests using the HFU concept. As an example, a geospatial model-based hybridization of Shannon's entropy and the TOPSIS algorithm was developed for map-

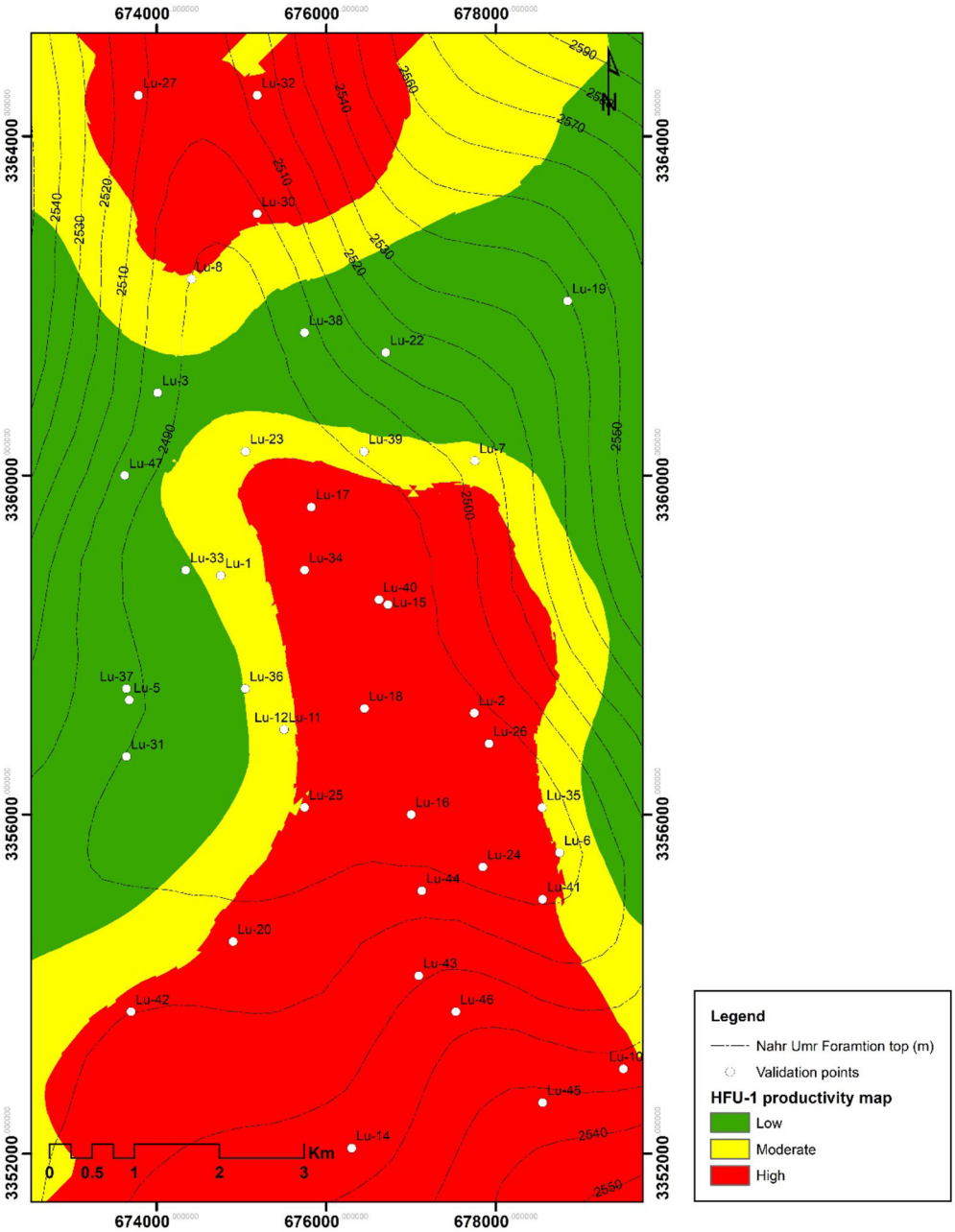

Fig. 8. HFU-1 productivity map (middle Nahr Umr Formation).

ping hydrocarbon productivity in the middle reservoir unit of the Nahr Umr Formation in the Luhais oil field, southern Iraq. The objective of the exercise was to delineate which portion of the reservoir unit was highly productive in order to imitate a drilling exploration program. The main results were as follows. (1) The middle part of the Nahr Umr reservoir unit is heterogeneous. (The average calculated L_k and V_k were 0.65 and 0.93, respectively.) (2) The reservoir unit can be characterized by two HFUs based on the results of the k-means clustering technique. (3) The ranked values using the TOPSIS approach were classified into three hydrocarbon productivity zones using the geometric classification

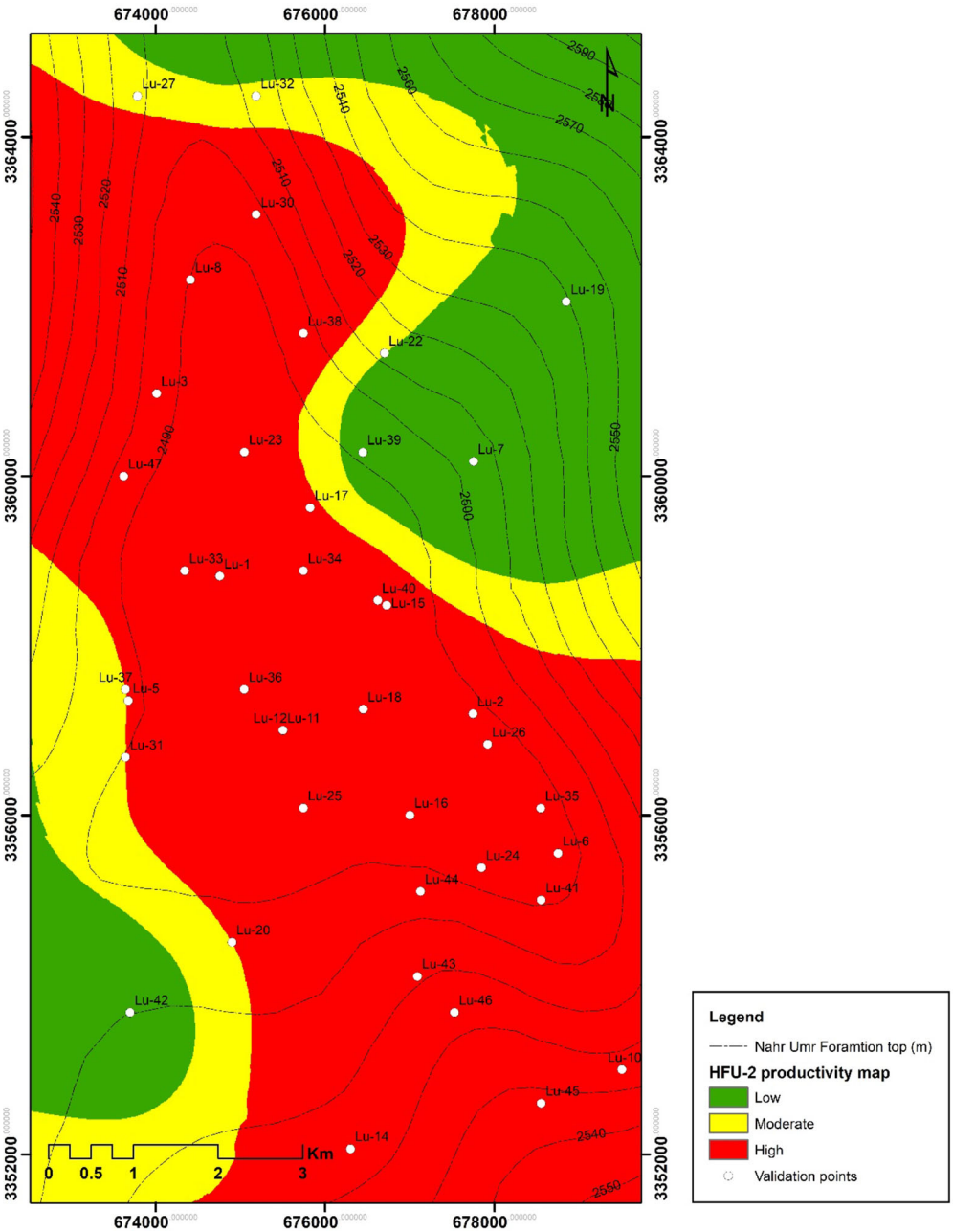

Fig. 9. HFU-2 productivity map (middle Nahr Umr Formation).

scheme of low-, moderate-, and high-productivity zones. These zones occupy 32, 22, and 45 km^2 for the low-, moderate-, and high-productivity zones, respectively, in the case of HFU-1; In contrast, the productivity zones extend over 30, 23, and 46 km^2 of the study area, respectively, for HFU-2. (4) The moderate- to high-productivity zones for HFU-1 and HFU-2 encompass 77% and 70% of the study area, respectively, indicating that the middle reservoir unit is promising in terms of hydrocarbon productivity. (5) In the case of the spatial distribution of the productivity zones, the high-productivity hydrocarbon zone occurs in the southern and northern parts of HUF-1 and in a northeast–southeast swath across

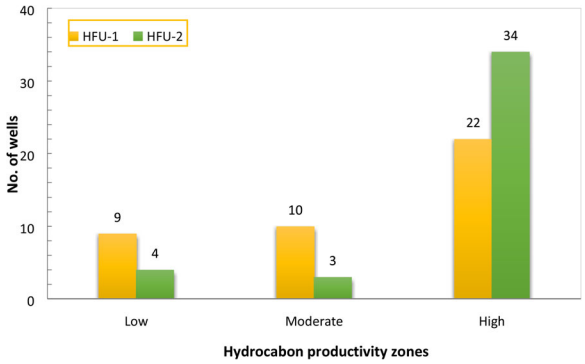

Fig. 10. Validation of the model results.

middle part of HFU-2. (6) The lower part of the Nahr Umr reservoir unit is more productive than the upper one. (7) Comparing the already productive wells in the field with the deduced productivity zones indicates that the developed TOPSIS models performed well with 76% and 88% for the HUF-1 TOPSIS and HFU-2 TOPSIS models, respectively. (8) It is clear that the productivity maps developed in this study can be used for efficient management of reservoirs and as guides for drilling new, highly productive wells with minimum effort and cost.

Finally, it is important to note that the accuracy of the developed models can be enhanced in the future by incorporating more petrophysical factors, like permeability, if data were available, and more advanced techniques, such as soft computing and machine learning techniques, can be used for building even more accurate models.

REFERENCES

Abdullah, F. H. A., Nederlof, P. J. R., Ormerod, M. P., & Kinghorn, R. R. F. (1997). Thermal history of the lower and middle cretaceous source rocks in Kuwait. *GeoArabia, 2*(2), 151–164.

Abid, N. J., Al-Shaikhly, S. S., & Al-Zaidy, A. A. H. (2015). Facies architecture and diagenetic features development of Albian-Early Turonian succession in Luhais oil field, Southern Iraq. *Iraqi Journal of Science, 56*(3B), 2308–2320.

Al-Abadi, A. M., & Al-Ali, A. K. (2018). Susceptibility mapping of gully erosion using GIS-based statistical bivariate models: a case study from Ali Al-Gharbi District, Maysan Governorate, southern Iraq. *Environmental Earth Sciences*. https://doi.org/10.1007/s12665-018-7434-2.

Al-Abadi, A. M., Al-Kubaisi, Q. Y., & Al-Ghanimy, M. A. (2018). Mapping groundwater zones contaminated by hydrocarbons in the Dammam aquifer in the Karbala-Najaf plateau, Iraq. *Environmental Earth Sciences, 77*(18), 633.

Al-Abadi, A. M., & Al-Najar, N. A. (2019). *Comparative assessment of bivariate, multivariate and machine learning models for mapping flood proneness. Natural Hazards*. Netherlands: Springer. https://doi.org/10.1007/s11069-019-03821-y.

Al-Abadi, A. M., Handhal, A. M., & Al-Ginamy, M. A. (2019). Evaluating the Dibdibba aquifer productivity at the Karbala-Najaf Plateau (Central Iraq) using GIS-based tree machine learning algorithms. *Natural Resources Research*. https://doi.org/10.1007/s11053-019-09561-x.

Al-Naqib, K. M. (1967). Geology of the Arabian peninsula. *USGS Professional paper No*.

Alshayef, M. S., Javed, A., & Mohammed, A. M. B. (2019). Delineation of hydrocarbon potential zones in Masila oil field, Yemen. *Spatial Information Research, 27*(2), 121–135. https://doi.org/10.1007/s41324-018-0220-0.

Amaefule, J. O., Altunbay, M., Tiab, D., Kersey, D. G., & Keelan, D. K. (1993). Enhanced reservoir description: using core and log data to identify hydraulic (flow) units and predict permeability in uncored intervals/wells. In *SPE annual technical conference and exhibition*. Society of Petroleum Engineers.

Amiri, M. A., Karimi, M., & Sarab, A. A. (2015). Hydrocarbon resources potential mapping using evidential belief functions and frequency ratio approaches, southeastern Saskatchewan, Canada. *Canadian Journal of Earth Sciences, 52*(3), 182–195. https://doi.org/10.1139/cjes-2013-0193.

Aqrawi, A. A. M., Mahdi, T. A., Sherwani, G. H., & Horbury, A. D. (2010). Characterisation of the Mid-Cretaceous mishrif reservoir of the southern Mesopotamian Basin, Iraq. In *American Association of Petroleum Geologists Conference and Exhibition* (Vol. 7, pp. 7–10).

Arabameri, A., Pradhan, B., Rezaei, K., & Conoscenti, C. (2019). Gully erosion susceptibility mapping using GIS-based multicriteria decision analysis techniques. *CATENA, 180*(April), 282–297. https://doi.org/10.1016/j.catena.2019.04.032.

Assari, A., & Assari, E. (2012). Role of public participation in sustainability of historical city: Usage of TOPSIS method. *Indian Journal of Science and Technology, 5*(3), 2289–2294.

Azareh, A., Rahmati, O., Rafiei-Sardooi, E., Sankey, J. B., Lee, S., Shahabi, H., et al. (2019). Modelling gully-erosion susceptibility in a semi-arid region, Iran: Investigation of applicability of certainty factor and maximum entropy models. *Science of the Total Environment, 655,* 684–696. https://doi.org/10.1016/j.scitotenv.2018.11.235.

Bingham, L., Zurita-Milla, R., & Escalona, A. (2012). Geographic information system-based fuzzy-logic analysis for petroleum exploration with a case study of northern South America. *AAPG Bulletin, 96*(11), 2121–2142. https://doi.org/10.1306/04251212009.

Bui, D. T., Shirzadi, A., Chapi, K., Shahabi, H., Pradhan, B., Pham, B. T., et al. (2019). A hybrid computational intelligence approach to groundwater spring potential mapping. *Water (Switzerland), 11*(10), 1–30. https://doi.org/10.3390/w11102013.

Charrad, M., Ghazzali, N., Boiteau, V., & Niknafs, A. (2012). *NbClust package: Finding the relevant number of clusters in a dataset*. Softw: Journal of Statistical.

Chen, Z., & Osadetz, K. G. (2005). Simulating the spatial distribution of undiscovered petroleum accumulations. *Journal of Canadian Petroleum Technology, 44*(3), 24–30. https://doi.org/10.2118/05-03-01.

Chen, W., Xie, X., Peng, J., Shahabi, H., Hong, H., Bui, D. T., et al. (2018). GIS-based landslide susceptibility evaluation using a novel hybrid integration approach of bivariate statistical based random forest method. *CATENA, 164,* 135–149. https://doi.org/10.1016/j.catena.2018.01.012.

Darweesh, H. A., Obed, A. Z. M., & Albadran, B. N. (2017). Structural study of basins configuration in mesopotamian area. *International Journal of Engineering and Applied Sciences*, *4*(9), 54–58.

De Smith, M. J., Goodchild, M. F., & Longley, P. (2007). *Geospatial analysis: a comprehensive guide to principles, techniques and software tools*. Kibworth Harcourt: Troubador Publishing Ltd.

Ditmar, V., & Team, I.-S. (1972). Geological conditions and hydrocarbon prospects of the republic of Iraq. Vol. 11, South Iraq. *Manuscript report, INOC Library, Baghdad, Iraq*.

Dou, J., Yunus, A. P., Bui, D. T., Merghadi, A., Sahana, M., Zhu, Z., et al. (2019). Improved landslide assessment using support vector machine with bagging, boosting, and stacking ensemble machine learning framework in a mountainous watershed, Japan. *Landslides*, https://doi.org/10.1007/s10346-019-01286-5.

Dunnington, H. V., Wetzel, R., & Morton, D. M. (1959). Mesozoic and Palaeozoic. *Lexique Stratigraphique International, 3,* 1–133.

Ebanks Jr, W. J. (1987). Flow unit concept-integrated approach to reservoir description for engineering projects. *AAPG (Am. Assoc. Pet. Geol.) Bull.;(United States)*, *71*(CONF-870606-).

Ellis, D. V., & Singer, J. M. (2007). *Well logging for earth scientists* (Vol. 692). Berlin: Springer.

Fouad, S. F. A. (2010). Tectonic and structural evolution of the Mesopotamia Foredeep, Iraq. *Iraqi Bulletin of Geology and Mining, 6*(2), 41–53.

Gao, H., Chen, Z., Osadetz, K. G., Hannigan, P., & Watson, C. (2000). A pool-based model of the spatial distribution of undiscovered petroleum resources. *Mathematical Geology, 32*(6), 725–749. https://doi.org/10.1023/A:1007594423172.

Goodchild, M. F. (2005). GIS and modeling overview. *GIS, spatial analysis, and modeling. ESRI Press, Redlands*, 1–18.

Gunter, G. W., Finneran, J. M., Hartmann, D. J., & Miller, J. D. (1997). Early determination of reservoir flow units using an integrated petrophysical method. In *SPE annual technical conference and exhibition*. Society of Petroleum Engineers.

Hafezalkotob, A., & Hafezalkotob, A. (2016). Extended MULTIMOORA method based on Shannon entropy weight for materials selection. *Journal of Industrial Engineering International, 12*(1), 1–13.

Handhal, A. M. (2016). The spatial analysis of Yamama Formation heterogeneity in south of Iraq. *Iraqi Journal of Science, 57*(3A), 1783–1794.

Hearn, C. L., Ebanks, W. J., Jr., Tye, R. S., & Ranganathan, V. (1984). Geological factors influencing reservoir performance of the Hartzog draw field, Wyoming. *Journal of Petroleum Technology, 36*(08), 1–335.

Husseini, M. I. (1988). The Arabian infracambrian extensional system. *Tectonophysics, 148*(1–2), 93–103.

Hwang, C.-L., & Yoon, K. (1981). Methods for multiple attribute decision making. In *Multiple attribute decision making* (pp. 58–191). Springer.

Ibrahim, M. W. (1983). Petroleum geology of southern Iraq. *AAPG Bulletin, 67*(1), 97–130.

Idan, R. M., Al-Musawi, F. A., & Salih, A. L. (2019). The petroleum system of Zubair Formation in Zubair subzone, southern Iraq. *Journal of Petroleum Reserach and Studies, 12*(25), 57–73.

James, G. A., & Wynd, J. G. (1965). Stratigraphic nomenclature of Iranian oil consortium agreement area. *AAPG Bulletin, 49*(12), 2182–2245.

Janizadeh, S., Avand, M., Jaafari, A., Van Phong, T., Bayat, M., Ahmadisharaf, E., et al. (2019). Prediction success of machine learning methods for flash flood susceptibility mapping in the Tafresh watershed, Iran. *Sustainability (Switzerland), 11*(19), 1–19. https://doi.org/10.3390/su11195426.

Jassim, S Z, & Goff, J. C. (2006). Geology of Iraq. Dolin, prague and moravian museum. *Brno*, p. 341.

Jenks, G. F. (1967). The data model concept in statistical mapping. *International Yearbook of Cartography, 7,* 186–190.

Jensen, J., Lake, L. W., Corbett, P. W. M., & Goggin, D. (2000). *Statistics for petroleum engineers and geoscientists* (Vol. 2). Houston: Gulf Professional Publishing.

Kordestani, M. D., Naghibi, S. A., Hashemi, H., Ahmadi, K., Kalantar, B., & Pradhan, B. (2019). Groundwater potential mapping using a novel data-mining ensemble model. *Hydrogeology Journal, 27*(1), 211–224. https://doi.org/10.1007/s10040-018-1848-5.

Lefohn, A. S., Knudsen, H. P., & Shadwick, D. S. (2005). Using ordinary kriging to estimate the seasonal W126, and N100 24-h concentrations for the Year 2000 and 2003. *ASL & Associates*, *111*.

Liu, H. (2017). *Principles and applications of well logging*. Berlin: Springer.

Liu, X., Zhong, G., Yin, J., He, Y., & Li, X. (2008). GIS-based modeling of secondary hydrocarbon migration pathways and its application in the northern Songliao Basin, northeast China. *Computers & Geosciences, 34*(9), 1115–1126. https://doi.org/10.1016/j.cageo.2007.08.005.

MacQueen, J. (1967). Some methods for classification and analysis of multivariate observations. In *Proceedings of the fifth Berkeley symposium on mathematical statistics and probability* (Vol. 1, pp. 281–297). Oakland, CA, USA.

Maguire, D. J., Batty, M., & Goodchild, M. F. (2005). *GIS, spatial analysis, and modeling*. Redlands: Esri Press.

Nohani, E., Moharrami, M., Sharafi, S., Khosravi, K., Pradhan, B., Pham, B. T., et al. (2019). Landslide susceptibility mapping using different GIS-Based bivariate models. *Water (Switzerland), 11*(7), 1–22. https://doi.org/10.3390/w11071402.

Orodu, O. D., Tang, Z., & Fei, Q. (2016). Hydraulic (Flow) unit determination and permeability prediction: A case study of block Shen-95, Liaohe Oilfield, North_East China. *Journal of Applied Sciences, 9*(10), 1801–1816.

Owen, R. M. S., & Nasr, S. N. (1958). Stratigraphy of the Kuwait-Basra area: Middle East.

Polatidis, H., Haralambopoulos, D. A., Munda, G., & Vreeker, R. (2006). Selecting an appropriate multi-criteria decision analysis technique for renewable energy planning. *Energy Sources, Part B: Economics, Planning and Policy, 1*(2), 181–193. https://doi.org/10.1080/009083190881607.

Powers, R. W. (1968). Lexique stratigraphique international. Vol. III, Asie, Fas. 10 b1, Arabia Saoudite. *CNRS, Paris*.

Qaradaghi, A. I., Abdul-Kareem, B. M., & Al-Jassim, J. A. (2008). Petrography, diagenesis and depositional environment of Nahr Umr Formation, from selected wells in central Iraq. *Iraqi Bulletin of Geology and Mining, 4*(1), 67–94.

Rad, J. R., Derakhshani, R., Farhoudi, G., & Ghorbani, H. (2008). Basement faults and salt plug emplacement in the arabian platform in Southern Iran. *J. Appl. Sci, 8*(18), 3235–3241.

Rudini Matori, A. N., Ab Talib, J., & Balogun, A. L. (2018). Application of geographic information system (GIS) to model the hydrocarbon migration: Case study from North-East Malay Basin, Malaysia. *E3S Web of Conferences*. https://doi.org/10.1051/e3sconf/20183402027.

Shannon, C. E. (1948). A mathematical theory of communication. *Bell System Technical Journal, 27*(3), 379–423.

Siahaan, A. P. U., Rahim, R., & Listyorini, T. (2018). TOPSIS method application for decision support system in internal control for selecting best employees.

Tiab, D., & Donaldson, E. C. (2015). *Petrophysics: theory and practice of measuring reservoir rock and fluid transport properties*. Houston: Gulf Professional Publishing.

van Bellen, R. C., Dunnington, H. V., Wetzel, R., & Morton, D. M. (1959). *Lexique stratigraphique international Asia, fascicule, 10a, Iraq* (p. 33). Paris: Center National de la Recherché Scientifique.

Wind, Y., & Saaty, T. L. (1980). Marketing applications of the analytic hierarchy process. *Management Science, 26*(7), 641–658.

Yamamoto, J. K. (2005). Comparing ordinary kriging interpolation variance and indicator kriging conditional variance for assessing uncertainties at unsampled locations. *Application of computers and operations research in the mineral industry– Dessureault, Ganguli, Kecojevic, & Dwyer editors, Balkema.*

Yue, C. (2017). Entropy-based weights on decision makers in group decision-making setting with hybrid preference representations. *Applied Soft Computing, 60,* 737–749.